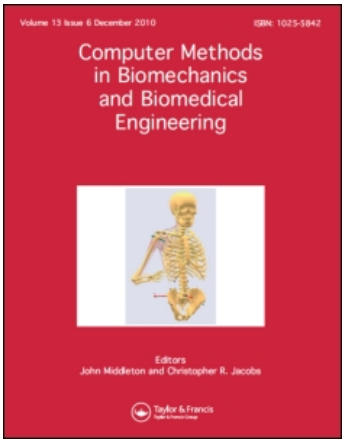

Computer Methods in Biomechanics and Biomedical Engineering
Publication details, including instructions for authors and subscription information:
http://www.informaworld.com/smpp/title~content=t713455284

Towards automatic quantification of the epicardial fat in non-contrasted CT images

Jorge G. Barbosa[a]; Bruno Figueiredo[a]; Nuno Bettencourt[b]; João Manuel R. S. Tavares[c]
[a] Laboratório de Inteligência Artificial e Ciência dos Computadores, Departamento de Engenharia Informática, Faculdade de Engenharia, Universidade do Porto, Porto, Portugal [b] Departmento de Cardiologia, Centro Hospitalar de Gaia, V.N. Gaia, Portugal [c] Departamento de Engenharia Mecânica, Faculdade de Engenharia, Universidade do Porto/Instituto de Engenharia Mecânica e Gestão Industrial - Rua Dr. Roberto Frias, Porto, Portugal

First published on: 10 March 2011

To cite this Article Barbosa, Jorge G. , Figueiredo, Bruno , Bettencourt, Nuno and Tavares, João Manuel R. S.(2011) 'Towards automatic quantification of the epicardial fat in non-contrasted CT images', Computer Methods in Biomechanics and Biomedical Engineering,, First published on: 10 March 2011 (iFirst)
To link to this Article: DOI: 10.1080/10255842.2010.499871
URL: http://dx.doi.org/10.1080/10255842.2010.499871

Computer Methods in Biomechanics and Biomedical Engineering
iFirst article, 2011, 1–10

Taylor & Francis
Taylor & Francis Group

Towards automatic quantification of the epicardial fat in non-contrasted CT images

Jorge G. Barbosa[a]*, Bruno Figueiredo[a], Nuno Bettencourt[b] and João Manuel R.S. Tavares[c]

[a]*Laboratório de Inteligência Artificial e Ciência dos Computadores, Departamento de Engenharia Informática, Faculdade de Engenharia, Universidade do Porto, Porto, Portugal;* [b]*Departmento de Cardiologia, Centro Hospitalar de Gaia, V.N. Gaia, Portugal;* [c]*Departamento de Engenharia Mecânica, Faculdade de Engenharia, Universidade do Porto/Instituto de Engenharia Mecânica e Gestão Industrial – Rua Dr. Roberto Frias, 4200-465 Porto, Portugal*

(*Received 9 April 2010; final version received 7 June 2010*)

In this work, we present a technique to semi-automatically quantify the epicardial fat in non-contrasted computed tomography (CT) images. The epicardial fat is very close to the pericardial fat, being separated only by the pericardium that appears in the image as a very thin line, which is hard to detect. Therefore, an algorithm that uses the anatomy of the heart was developed to detect the pericardium line via control points of the line. From the points detected an interpolation was applied based on the cubic interpolation, which was also improved to avoid incorrect interpolation that occurs when the two variables are non-monotonic. The method is validated by using a set of 40 CT images of the heart of 40 human subjects. In 62.5% of the cases only minimal user intervention was required and the results compared favourably with the results obtained by the manual process.

Keywords: anatomical model-based segmentation; clustering; low-contrasted images; polynomial interpolation

1. Introduction

Obesity is recognised as an important risk factor for the development of cardiovascular disease (Hubert et al. 1983; Manson et al. 1990; Visscher et al. 2001). The quantification of visceral fat (fat surrounding the internal viscera), in contrast to the subcutaneous fat (deposited under the skin), has been shown to correlate closely with the development of atherosclerotic diseases and with the parameters of the metabolic syndrome. Therefore, some methods (Jeong et al. 2007) have been developed in order to quantify the non-invasive fat composition, assessing the total body fat and visceral tissue. The visceral abdominal tissue is used for quantification of visceral fat and Borkan et al. (1982) described a method for performing this quantification using computed tomography (CT) image data.

The epicardial fat, the object of this study, is a deposition of visceral fat that surrounds the heart, accumulating mainly in the atrioventricular and interventricular grooves surrounding the epicardial coronary arteries (Manson et al. 1990). Not much is known about the true role and metabolic pathophysiology of epicardial fat; however, recent data have suggested its involvement in the development and progression of coronary atherosclerosis (Iacobellis et al. 2005). Epicardial fat produces numerous cytokines and proteins associated with atherosclerosis (Mazurek et al. 2003). This coupled with the lack of a real anatomical barrier between the tissue and the coronary arteries suggests a pro-atherogenic effect directly on the vessels.

The method presented here addresses the problem of measuring the epicardial fat in non-contrasted CT images, which is more difficult to measure than contrasted images. The results show that the method is an improvement on the traditional manual procedure by requiring less interaction of a technician as well as by reducing the variability of the results. Section 2 describes the quantification of the fat on the heart using CT images. Section 3 analyses image content in CT images. Section 4 reviews image segmentation techniques. Section 5 describes the proposed method for epicardial fat quantification. Section 6 presents results and Section 7 conclusions.

2. Related work

CT has been used to quantify visceral fat for a long time now. This evaluation is carried out using a single cut of the abdominal CT. Along with recent developments in CT and applications to the region of the heart, there has been an increasing interest in quantifying the deposition of fat on the heart. Some quantification processes have been applied as shown by Gorter et al. (2008). However, these processes are mostly manual requiring significant post-processing time. Attempts to automate this task have had some success and it is possible to quantify pericardial fat automatically, as described by Dey et al. (2008). However,

*Corresponding author. Email: jbarbosa@fe.up.pt

ISSN 1025-5842 print/ISSN 1476-8259 online

DOI: 10.1080/10255842.2010.499871
http://www.informaworld.com

these methods measure the total fat on the heart, without distinguishing the epicardial fat.

Clinical practice today uses either an automatic measurement of the total fat without distinguishing the epicardial one, or a manual segmentation method where an operator selects points from the image belonging to the pericardium that are then connected by a first-order segment (Bandekar et al. 2006).

Due to the clinical interest in epicardial fat measurements (see de Vos et al. 2008) and due to the lack of a method that allows its automatic or semiautomatic quantification, this paper presents a novel method that in some cases can quantify the epicardial fat automatically and in others requires only a minimal user intervention.

To the best of our knowledge, this is the first method proposed to compute the epicardial fat in non-contrasted CT images; preliminary results of this method were presented by Figueiredo et al. (2009).

3. Non-contrasted CT image data

The images obtained by CT have, in general, a resolution of 12 bits per pixel, allowing 4096 grey levels which in CT represents numbers ranging from −1000 to 3095. This grey scale was created especially for CT imaging and is called Hounsfield units (HU). On this scale, as shown in Figure 1, water has a value of 0 HU, air −1000 HU, the cortical bone +1000 HU and the fat occupies a range of around −100 HU according to Borkan et al. (1982) and Yoshizumi et al. (1999).

The distinction between fat and other tissues is made through different levels of attenuation of the different tissues and consequently through HU in the image. There are several studies (Borkan et al. 1982; Yoshizumi et al. 1999) published on the correlation between HU and fat deposition. These studies indicate that fat has a density between −50 and −150 HU, or between −30 and −190 HU. In this research and following other publications on the quantification of fat, specifically in the heart (Dey et al. 2008), the range of −30 to −190 HU was used.

The image from the non-contrasted CT is shown in Figure 2. The pericardium appears as a thin line,

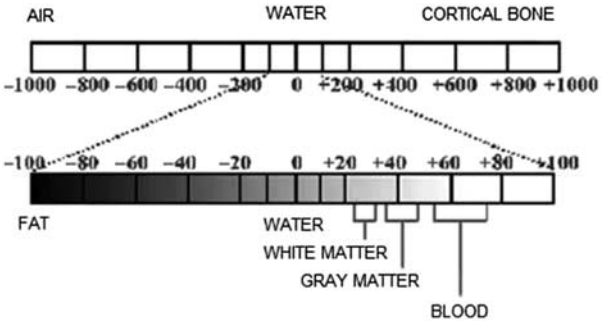

Figure 1. HU scale.

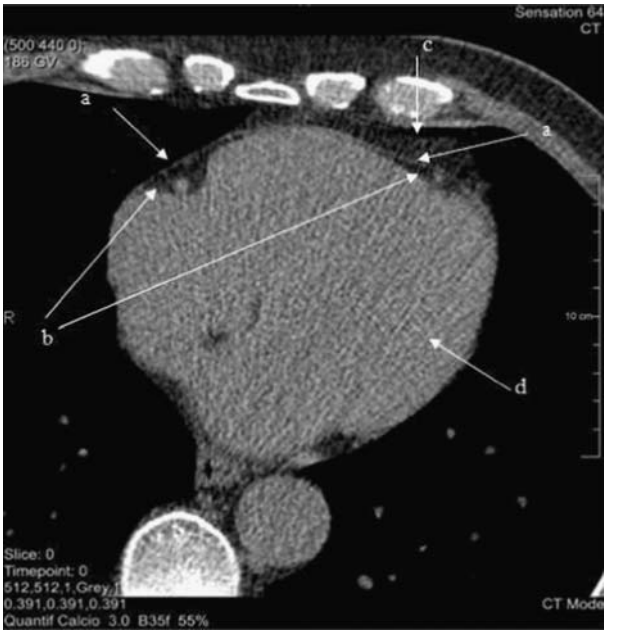

Figure 2. Original image: (a) the pericardium; (b) the epicardial fat; (c) the pericardial fat and (d) muscle and cardiac cavities.

identifiable mainly at the anterior region of the heart, as shown by (a) labels. Label (d) represents the region that includes the muscle and the heart chambers. Labels (b) represent the epicardial fat and label (c) is the adipose tissue. These later regions of fat are very close to each other and only the pericardium which is a very thin barrier separates them. It is not always easy to identify and follow the pericardium throughout its full length due to its thinness.

To evaluate the possibility of segmenting the pericardium based on HU, a set of 104 samples was taken from a set of 10 images. Also a set of 100 samples was taken for the cardiac muscle from the same 10 images. Figure 3 shows the values obtained for each structure. Statistically, the pericardium samples have a mean of −13 HU and a standard deviation of 31 HU; the cardiac muscle samples have a mean of 38 HU and a standard deviation of 23 HU. The Pericardium is closer to the fat intensities that are in the −30 to −190 HU range.

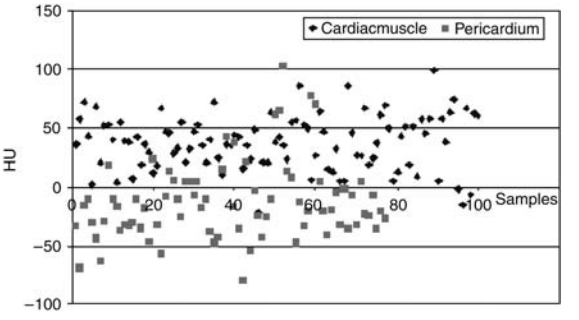

Figure 3. Intensity values in HU for a set of samples of the pericardium and cardiac muscle.

On an average, the cardiac muscles have higher intensity than the pericardium; however, there is a substantial overlap that prevents an automatic method to be based on intensity segmentation. Once the pocket of fat separates the cardiac muscle from the pericardium, if one starts a region growing algorithm (Pham et al. 2000; Ma et al. 2010) inside the cardiac muscle, it will stop on the pericardium fat, without joining the pericardium pixels. This approach is used in the algorithm presented in Section 5.

In the process to quantify the epicardial fat today, the pericardial line is selected manually. However that line is often not visible for its full length and, therefore, the operator has to connect several short pericardium segments, and guess some points, in order to delineate the line fully. Obviously, there is an intrinsic error associated to this procedure and, therefore, an experiment to quantify the inter-observer variability was carried out. A set of 40 images were segmented for epicardial fat quantification by 3 expert operators. Table 1 shows individual results and the mean value of fat for each image.

For each image I_i, with $1 \leq i \leq 40$, the mean measurements among operators $\overline{m_i}$ was computed; and for each operator j, for $j = \{1, 2, 3\}$, the relative error is given by $e_{ji} = (m_{ji} - \overline{m_i})/\overline{m_i}$. The measurement of image I_i by operator j was m_{ji}. The mean relative error of all $e_{ji} = 5.6\%$ and standard deviation $= 4.8\%$. This results in a maximum inter-operators relative deviation of 10.4%.

We concluded that the present procedures for epicardial fat quantification can have differences among operators as high as 10.4%. Therefore, on evaluating the results of the algorithm proposed in this paper, a result that differs up to 10.4% from the mean value obtained for each image ($\overline{m_i}$) is acceptable.

Table 1. Epicardial fat measured by three different operators.

Operator 1 (mm^2)	Operator 2 (mm^2)	Operator 3 (mm^2)	Mean (mm^2)
12,464	13,174	13,362	13,000
5790	5581	5790	5720
6224	6479	5916	6206
4996	5783	5271	5350
7322	8747	8048	8039
5713	5215	6264	5731
3594	4077	3647	3773
4145	4685	3551	4127
6094	6974	7087	6718
4980	7251	7212	6481
4592	6040	5714	5449
3886	3519	3591	3665
8463	10,133	9925	9507
4976	5079	5802	5286
8416	9423	9695	9178
11,465	13,137	16,845	13,816
8832	10,467	10,610	9970
2548	2705	2872	2708
8751	11,025	11,284	10,353
13,073	13,876	14,063	13,671
10,213	14,838	11,338	12,130
6463	7239	7053	6918
7506	7931	8679	8039
14,302	14,290	13,423	14,005
7217	6779	6651	6882
16,834	15,376	15,317	15,842
8493	8610	8153	8419
12,920	14,580	14,109	13,870
12,871	15,366	14,498	14,245
9897	11,288	10,608	10,598
9048	9011	9683	9247
1412	1465	1517	1464
831	946	1070	949
693	746	730	699
1154	984	1000	1045
1327	1443	1621	1461
1182	1119	1179	1159
1454	1531	1494	1492
3971	3889	4044	3968
1030	1017	1045	1051

4. Medical image segmentation techniques

Several surveys specific for medical image segmentation were published (Pham et al. 2000; Ma et al. 2010), classifying algorithms into several classes. Here, we consider three types of algorithms, namely, threshold techniques, clustering techniques and anatomical model-based segmentation, also called Atlas-guided segmentation.

4.1 Threshold techniques

These types of algorithms are based on the hypotheses that different structures, representing either organs or tissues, have different intensity levels or gradient magnitudes on the image, so that selecting pixels in a given range would result in the segmentation of a specific structure. This is especially applicable in high-contrasted images where the structures are well defined and have a significant homogeneous intensity. Figure 3 shows that the pericardium and the cardiac muscle have pixel intensities in the same range, which make the direct use of this technique difficult. Edge-based algorithms consider the gradient magnitude to segment structures, being successful in identifying intensity transitions that commonly occur at the border of structures. One widely used edge-detector algorithm is the Canny edge detector (Canny 1986). Figure 4 shows the result of this algorithm applied to a non-contrasted CT image. We can see that there are some well-delineated boundaries such as the heart shape but in the region of interest, in this case, the pericardium area, there is not a regular shape which makes the definition of a structure based only on this information difficult.

Another algorithm that belongs to the threshold technique class is the region growing algorithm as described by Adams and Bishop (1994). The algorithm

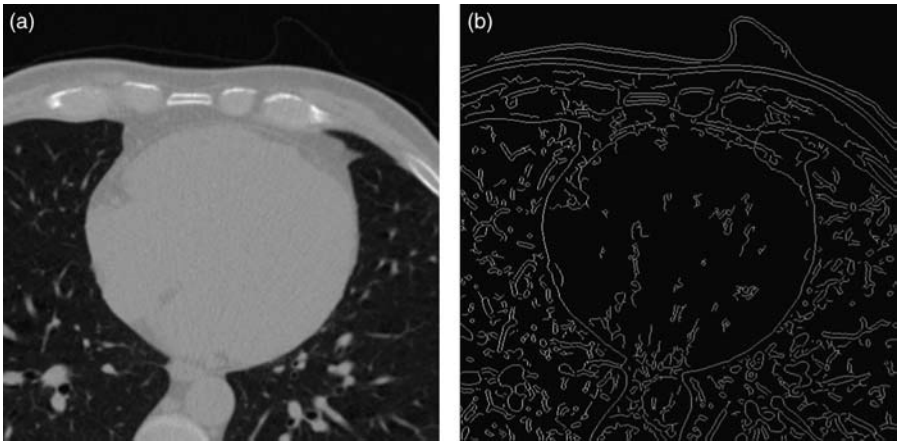

Figure 4. (a) Initial image; (b) edge detection with Canny algorithm.

selects pixels, in the neighbourhood of a seed pixel, which have the same intensity or only differ to a small specific amount. This is applied iteratively until no pixels are left. This is useful to identify structures that are homogeneous, with no texture or have small intensity differences in the interior compared with the structure of the boundaries. However, the structure must have a well-defined boundary in the image. This is the case of cardiac muscle that is surrounded by fat as shown in Figure 2. It will allow the removal of this structure from the image as explained in Section 5. The drawback of this algorithm is that it requires a seed pixel to start.

4.2 Clustering techniques

Clustering algorithms perform classification of data without using training data (Pham et al. 2000). They are designated as unsupervised classification techniques. Here, the *k*-means algorithm is used, *k* being the number of clusters to obtain in the result, to analyse the characteristics of the pericardium line in the image. The *k*-means algorithm was applied to the image where the cardiac muscle had been removed and we concluded that the pericardium line had the highest pixel values in the image. When classifying the pericaridum line in a different set of classes, it has the majority of its pixels in the last and higher intensity classes.

Figure 5(b) shows that using four classes, we cannot distinguish the pericardium data from the fat. With 20 classes, we can successfully isolate some pixels of the pericardium although other pixels are also selected. Figure 5(c) shows the 19 class of a 20 *k*-means segmentation. And Figure 5(d) shows the last class of the same segmentation. Clearly, class 20 is the one that contains the majority of the pericardium pixels. The algorithm proposed in this paper considers this characteristic.

4.3 Anatomical model-based segmentation

Anatomical model-based segmentation as described by Arata et al. (1995) uses anatomic knowledge to guide the segmentation. Currently, the model is constructed from several samples of the structures that we want to segment. Due to the variability of the sample data, the anatomic model is presented with statistical parameters in order to take into account the natural anatomic variation of the structure among human subjects. Here we used a simpler approach that is related to this technique, which consists of searching for points in the pericardium area that have the highest values, as explained below.

5. Fat quantification method

The process to measure epicardial fat automatically was separated into two steps. First, the image is preprocessed to remove any data that could interfere with the detection of the pericardium, and the second step is the segmentation of the pericardium and the subsequent quantification of fat.

The images in this study were first prepared following the method described by Dey et al. (2008) that removes all other structures apart from the heart, as shown in Figure 6(a).

5.1 Preprocessing algorithm

The preprocessing step of the algorithm to segment the pericardium is based on the fact that different tissues have different HU, mainly the fat and the muscle. The fat HUs are considered to range from -30 to -190 HU (Dey et al. 2008). Figure 7 shows the steps for the preprocessing algorithm. First, a region growing technique to detect the cardiac muscle is initiated with the centre pixel of the image as seed. If the seed is outside the intensity range of

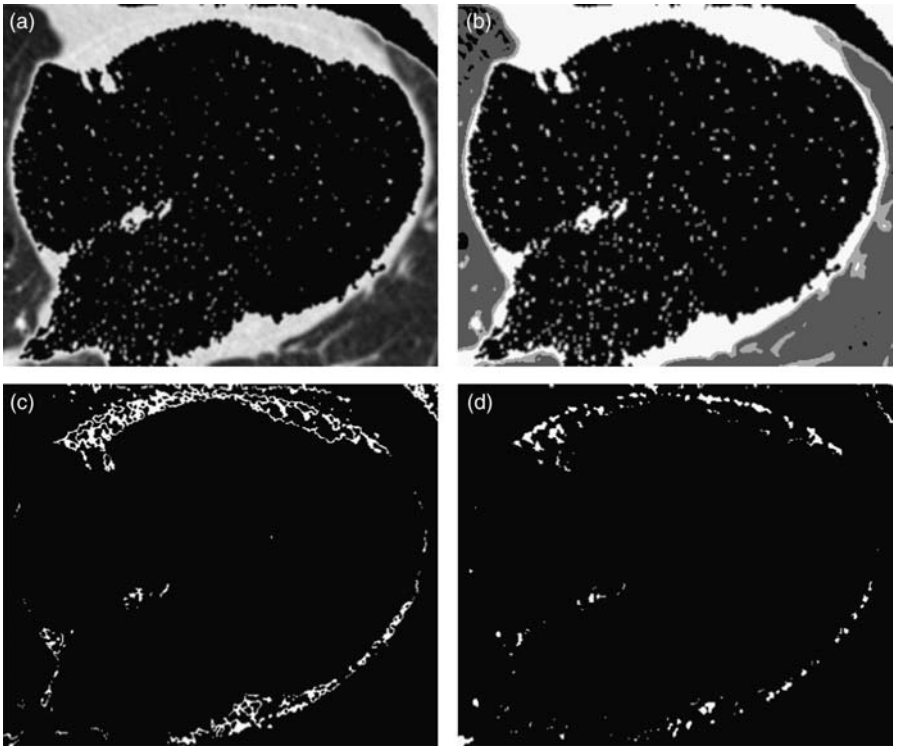

Figure 5. (a) Initial image; (b) *k*-means with four clusters; (c) cluster 19 of *k*-means with 20 clusters and (d) cluster 20 of *k*-means with 20 clusters.

the cardiac muscle then each pixel from the first line of eight neighbours are considered, sequentially, to be the seed. The process continues to the second line of neighbours and so forth until a pixel is in the intensity range required. The experience showed that the seed point is the centre pixel or one on the first line of neighbours. The second step consists in a threshold to remove high-intensity points because they do not represent the muscle but calcifications; the threshold removes points above 100 HUs. The third step uses a mean filter to reduce noise; a kernel of dimension 3×3 was used. Figure 6(b) shows the result of the region growing step that starts in the centre of the image and grows until it reaches the epicardial fat that has different intensities (HU). This pocket of fat also prevents the pericardium line from being removed. Figure 6(c) shows the image after removing the cardiac muscle. This image still has some artefacts that are removed by the threshold filter without affecting the fat and the pericardium line. Figure 6(d) shows the final result after applying the threshold and a mean filter for noise attenuation.

The pericardium is a very thin line on the image of Figure 6(d), which makes its segmentation difficult. Despite the great interest to quantify only the epicardial fat as described in Mazurek et al. (2003) there is no method to do it automatically. The pericardium is surrounded by fat that has lower intensity levels on the image. It is this difference in intensity, among other characteristics, such as the pericardial line being set mainly in the anterior region of the heart and its rounded appearance in the image that the segmentation algorithm is based.

5.2 Segmentation algorithm

According to the results shown in Figure 5(c) and (d), the higher values remaining in the image will belong mainly to the pericardium or the pixels surrounding it. With the reference in the centre of the image, the segmentation algorithm sweeps the anterior region from 0° to 180° registering the higher intensity points in each direction every 5° as shown in Figure 8(a). For each of these main directions the maximum point on the directions from $-5°$ to $+5°$ with a step of 1° is computed. From these points the mean and standard deviation of the coordinates are computed, as illustrated in Figure 8(b) where P_m is the mean position. Since the pericardium has no abrupt transitions, mean points that exceed a given standard deviation were rejected. In this study, the maximum standard deviation allowed for the P_m to belong to the Pericardium was found, experimentally, to be 10. Higher values would select points outside the pericardium and lower values would result, in most cases, in very few points being selected. Figure 9 shows the application of the algorithm.

Figure 9(a) shows the original image and Figure 9(b) the points detected. Only 15 points were selected to define

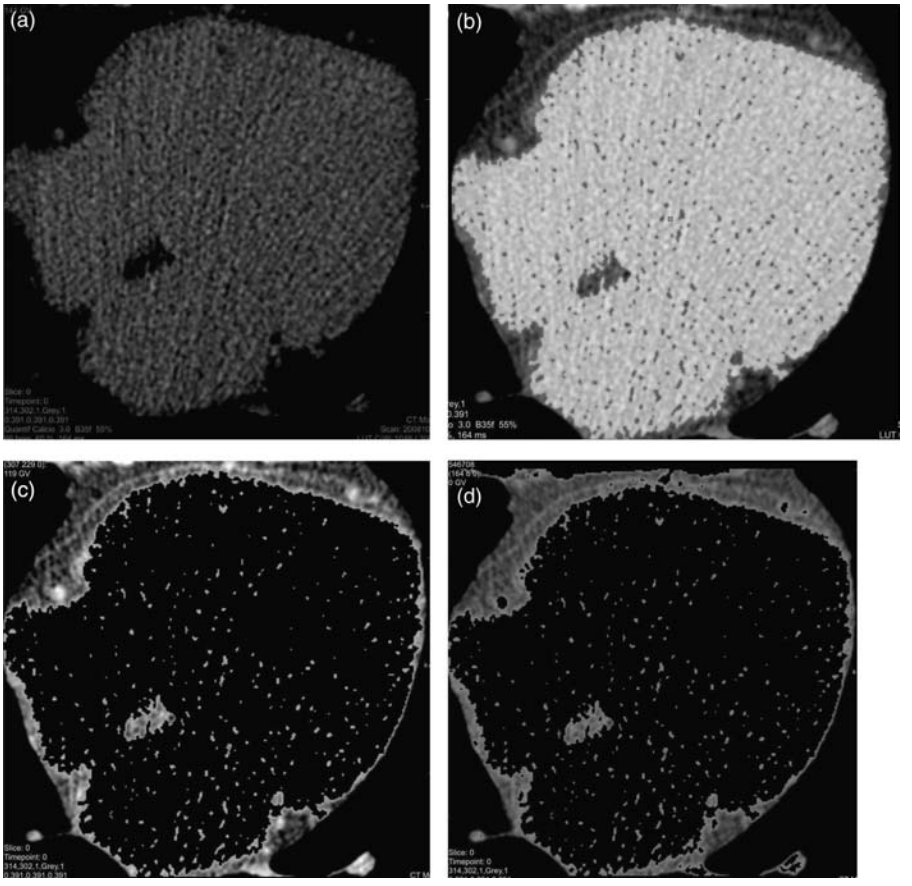

Figure 6. Preprocessing steps: (a) pre-selected image region; (b) muscle segmentation; (c) after muscle removal and (d) final image.

the pericardium. All others were rejected due to noise that results in standard deviations greater than 10. However, these 15 points are more than the minimum number required to define the pericardium line correctly as shown in Figure 9(c). This line is obtained by an improved spline interpolation that can deal with repeated values on both coordinates, as described below.

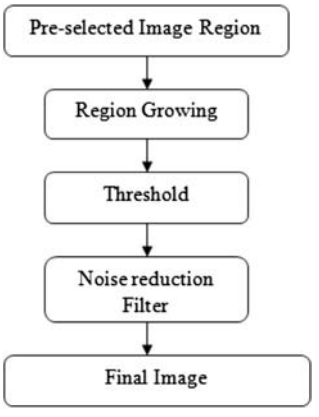

Figure 7. Preprocessing algorithm.

The fat quantification shown in Figure 9(d) is obtained by considering all pixels below the pericardium line with intensities in the fat range from -190 to -30 HU.

5.3 *Polynomial interpolation*

The set of points coming from the segmentation algorithm is sparse with irregular distances among them. A linear interpolation would require many more points than the ones coming from this process. The cubic interpolation is the alternative, since it can be applied to any set of consecutive points and has a second derivative greater than zero, allowing for the specification of smooth curves. The application of standard algorithms available in some software packages and described, for example, in Press et al. (1997) result in an erratic interpolation when the two variables are allowed to be non-monotonic as shown in Figure 10(a). The approach to overcome this problem was to represent the curve $y = f(x)$ parametrically as functions of the free parameter d: $y = f_1(d)$ and $x = f_2(d)$. The parameter d on a given (x_i, y_i) point is computed by the accumulated distance between points from the first one (x_0, y_0) to (x_i, y_i), given by $\sum_{j=1}^{i} \|(x_j, y_j) - (x_{j-1}, y_{j-1})\|$.

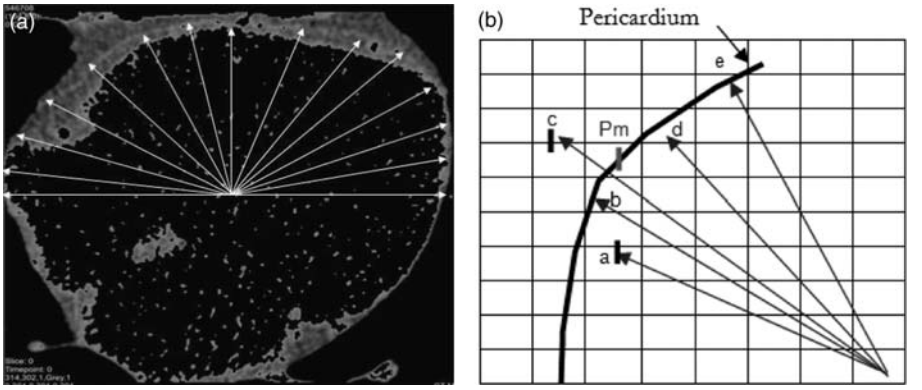

Figure 8. Pericardium segmentation: (a) detection of maximum values along a direction from the centre and (b) computation of a pericardium point.

Now, a standard cubic interpolation can be applied independently of the functions $y = f_1(d)$ and $x = f_2(d)$. The final curve shown in Figure 10(b) is obtained by computing (x, y) for a constant increment of d.

6. Results

The results of automatic quantification obtained were compared with results obtained manually, which were considered as reference values. However, a variability in the manual measurements of 10.4% was obtained for the same set of images by three different operators. This variability will be considered as the acceptable variability in the values automatically obtained when compared with the values of the manual procedure.

A set of 40 images was used to develop and test the algorithm. For training, 10 of these images were selected where the pericardium was clearly identifiable, but with different cardiac forms and distribution of fat. The results of this set are represented in Table 2. There are four images in which the system automatically detected the epicardial fat. In the other six cases, the system automatically

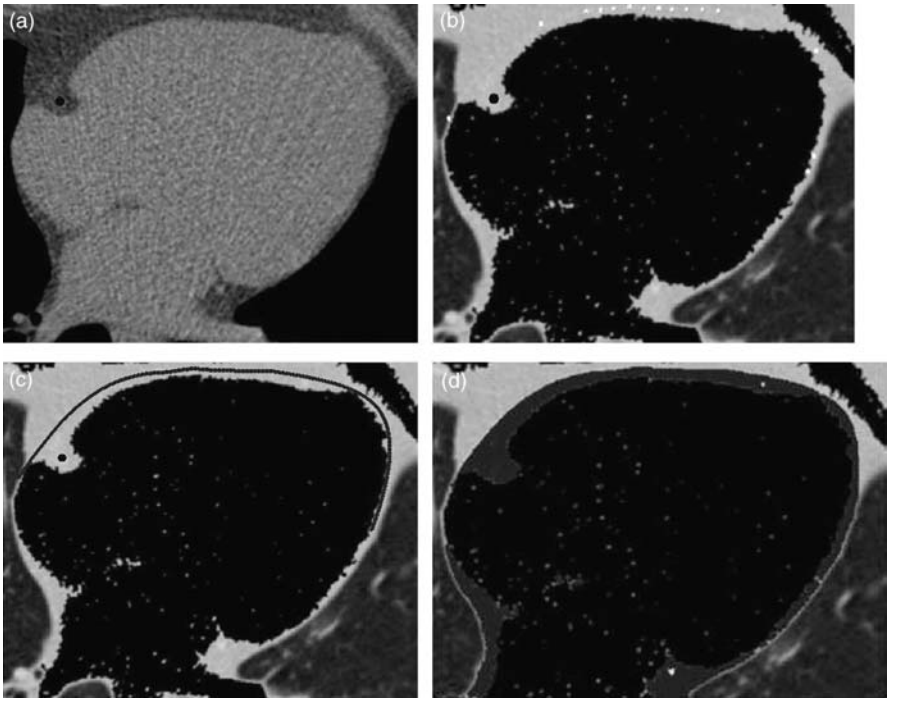

Figure 9. Pericardium segmentation: (a) initial image; (b) points detected; (c) pericardium line after spline interpolation and (d) fat quantification.

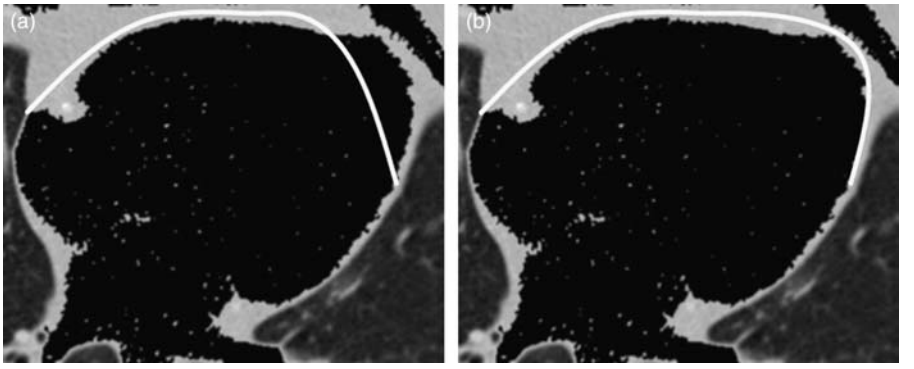

Figure 10. Pericardium interpolation: (a) standard cubic interpolation and (b) resulted cubic interpolation of $y = f_1(d)$ and $x = f_2(d)$.

detected much of epicardial fat although it needed a slight correction. With this minor alteration the system became well adjusted for the epicardial fat region. Table 2 compares the values obtained manually with the segmentation algorithm described here. The manual measurements are average values of three operators. The column of points adjusted shows the adjustment required by the user to obtain the presented result of the semi-automatic algorithm.

Figures 11 and 12 show the results from the set of 10 cases. In the first case, no correction was required to segment the pericardium correctly. In the second case, only two points were moved because they were trapped on a higher intensity region that did not represent the pericardium line.

The remaining 30 images were not used during training in order to have a set of new images to evaluate the effectiveness of the algorithm. In 11 images a maximum of 2 points required adjustment; 4 images required 3 points; and 2 images required 4 points to be adjusted. Visually the pericardium was very hard to identify in the other 13 images and consequently in most cases the algorithm did not identify any point of the pericardium or marked misplaced points. However, even in these cases the parametric cubic interpolation allows a faster and a more accurate manual segmentation than the actual linear one because it requires less points to be marked and describes the pericardium shape better. As shown in Figure 13 only seven points were sufficient to segment the pericardium.

7. Conclusions

Given the values obtained by the method presented in this paper, we conclude that this method is not suitable to operate in a fully automatic mode for all cases, since only four cases were detected automatically (10% of the cases). However, 52.5% of cases (21 out of 40) could be segmented correctly with a small adjustment by the user in setting up 2 or 3 points. The remaining cases consist of images where it is ambiguous for a technician to identify the pericardium line, which is the main reason for the variability of measurements among operators, as shown in Table 1; it is also the main limitation of the proposed method. That is, the method is not able to infer pericardium points from the heart anatomical model information, since its success is mainly dependent on pixel intensities.

The average error of the proposed method compared to the manual one is around 4%, for the semi-automatic segmentation (62.5% of cases). This is less than the deviation observed on the epicardial fat quantification

Table 2. Comparison between manual and semi-automatic method.

Image no.	Manual (mm^2)	Semi-auto (mm^2)	Difference (%)	Points adjusted
1	1221	1211	0.86	0
2	687	686	0.04	1
3	770	705	8.44	0
4	1384	1321	4.58	2
5	2379	2379	0.00	2
6	2580	2501	3.07	2
7	608	662	8.96	0
8	1087	1170	7.53	0
9	1376	1422	3.28	2
10	1684	1590	5.60	2

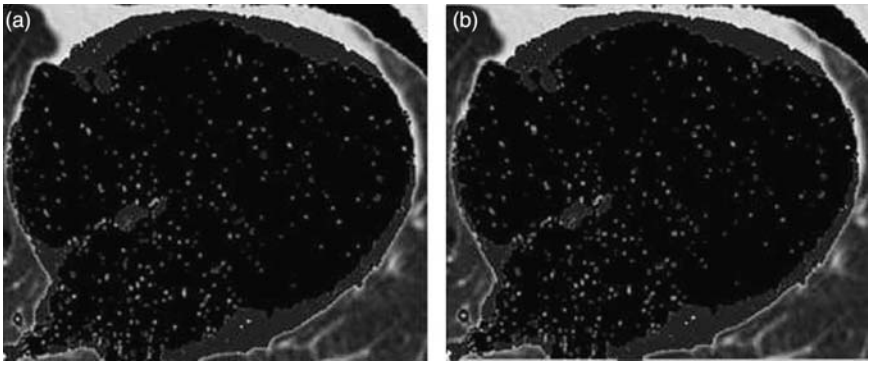

Figure 11. (a) Manual segmentation and (b) automatic segmentation.

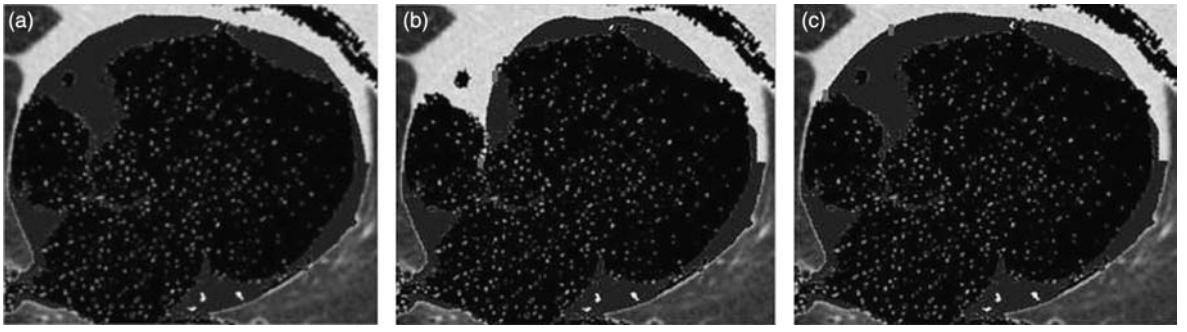

Figure 12. (a) Manual segmentation; (b) resulted cubic interpolation and (c) result after correction of two points.

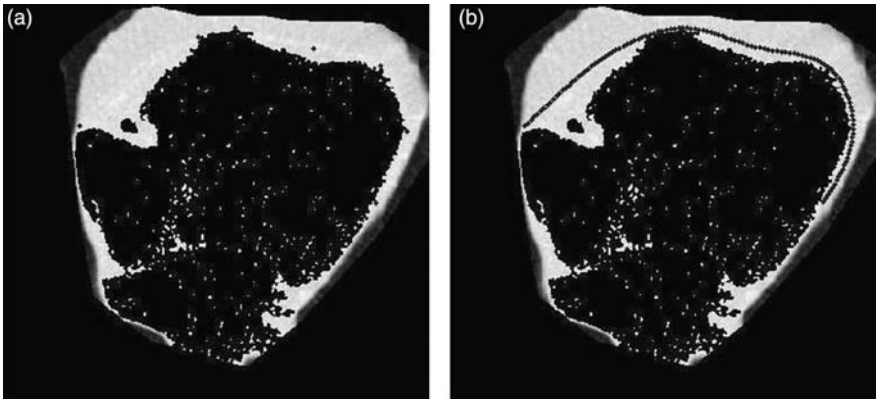

Figure 13. (a) Manual segmentation original image with seven points marked manually and (b) resulted cubic interpolation.

performed by different operators. There was a maximum deviation of 8.96%, compared to the 10.4% inter-operator.

From the images shown, we conclude that the automatic detection of the Pericardium on CT images without contrast is a very difficult problem. This is clear from the variations of the three operators when measuring the same set of images. To improve the results obtained, either manually or semi-automatically, we need to use higher level algorithms that, for example, use statistical data to define a starting pericardium line, which is then adapted using image data. It will also reduce user interaction even more by being able to infer pericardium points. However, statistic-based algorithms require a first step to collect data obtained by correct segmentations of the pericardium. We intend to use the method presented in this paper to feed a database of

pericardium shapes in order to apply statistical methods in our future work.

Even with the difficulties associated with the source images where the pericardium line is not clearly visible, the method proposed here allows an improvement in the procedure, since it requires less interaction by the technician and reduces the variability of results. Although the method requires user interaction, which is reduced to the last stage of the process to adjust a few points of the pericardium line, it should be pointed out that the method requires almost no parameter adjustments in any of its stages. In fact, the parameters of the preprocessing stage are simply based on HU of the tissues and in CT data, there is not the problem of light conditions as in the image acquisition, which is usually the main reason for such parameter adjustments. Thus, the segmentation algorithm stage may require the initial selection of the maximum standard deviation to be considered. However, the experience of this work showed that the value of 10 is a good trade off between correct identification of pericardium points and the identification of just a few points that would not represent the pericardium in all its extension.

Acknowledgements

This work was done partially in the scope of the projects: 'Methodologies to Analyze Organs from Complex Medical Images – Applications to Female Pelvic Cavity', 'Aberrant Crypt Foci and Human Colorectal Polyps: Mathematical Modelling and Endoscopic Image Processing' and 'Cardiovascular Imaging Modeling and Simulation – SIMCARD', with references PTDC/EEA-CRO/103320/2008, UTAustin/MAT/0009/2008 and UTAustin/CA/0047/2008, respectively, financially supported by Fundação para a Ciência e a Tecnologia in Portugal.

References

Adams R, Bishop L. 1994. Seeded region growing. IEEE Trans Pattern Anal Mach Intell. 16(6):641–647.

Arata LK, Dhawan AP, Broderick JP, Gaskil-Shipley MF, Levy AV, Volkow ND. 1995. Three-dimensional anatomical model-based segmentation of MR brain images through principal axes registration. IEEE Trans Biomed Eng. 42(11):1069–1078.

Bandekar AN, Naghavi M, Kakadiaris IA. 2006. Automated pericardial fat quantification in CT data. In: 28th IEEE EMBS annual international conference. New York: IEEE Computer Society. p. 932–935.

Borkan GA, Gerzof SG, Robbins AH, Hults DE, Silbert CK, Silbert JE. 1982. Assessment of abdominal fat content by computed tomography. Am J Clin Nutr. 36(1):172–177.

Canny J. 1986. A computational approach to edge detection. IEEE Trans Pattern Anal Mach Intell. 8(6):679–698.

de Vos AM, Prokop M, Roos JC, Meijs MFL, der Schouw YT, Rutten A, Gorter PM, Cramer M-J, Doevendans PA, Rensing BJ, Bartelink M-L, Velthuis BK, Mosterd A, Bots ML. 2008. Peri-coronary epicardial adipose tissue is related to cardiovascular risk factors and coronary artery calcification in post-menopausal women. Eur Heart J. 29(6):777–783.

Dey D, Suzuki Y, Suzuki S, Ohba M, Slomka PJ, Polk D, Shaw LJ, Berman DS. 2008. Automated quantitation of pericardiac fat from noncontrast CT. Invest Radiol. 43(2):145–153.

Figueiredo B, Barbosa JG, Bettencourt N, Tavares JMR. 2009. Semi-automatic quantification of the epicardial fat in CT images. In: VipIMAGE 2009 – II ECCOMAS Thematic Conference on Computational Vision and Medical Image Processing. p. 247–250.

Gorter PM, van Lindert ASR, de Vos AM, Meijs MFL, van der Graaf Y, Doevendans PA, Prokop M, Visseren FLJ. 2008. Quantification of epicardial and peri-coronary fat using cardiac computed tomography; reproducibility and relation with obesity and metabolic syndrome in patients suspected of coronary artery disease. Atherosclerosis. 197(2):896–903.

Hubert HB, Feinleib M, McNamara PM, Castelli WP. 1983. Obesity as an independent risk factor for cardiovascular disease: a 26-year followup of participants in the Framingham heart study. Circulation. 67(5):968–977.

Iacobellis G, Pistillic D, Gucciardo M, Leonetti F, Miraldi F, Brancaccio G, Gallo P, di Gioia CRT. 2005. Adiponectin expression in human epicardial adipose tissue *in vivo* is lower in patients with coronary artery disease. Cytokine. 29(6):251–255.

Jeong JW, Jeong MH, Yun KH, Oh SK, Park EM, Kim YK, Rhee SJ, Lee EM, Lee J, Yoo NJ, Kim NH, Park JC. 2007. Echocardiographic epicardial fat thickness and coronary artery disease. Circulation. 71(4):536–539.

Ma Z, Tavares J, Jorge R, Mascarenhas T. 2010. A review of algorithms for medical image segmentation and their applications to the female pelvic cavity. Comput Methods Biomech Biomed Eng. 13(2):235–246.

Manson JE, Colditz GA, Stampfer MJ, Willett WC, Rosner B, Monson RR, Speizer FE, Hennekens CH. 1990. A prospective study of obesity and risk of coronary heart disease in women. N Engl J Med. 322(13):882–889.

Mazurek T, Zhang L, Zalewski A, Mannion JD, Diehl JT, Arafat H, Sarov-Blat L, O'Brien S, Keiper EA, Johnson AG, Martin J, Goldstein BJ, Shi Y. 2003. Human epicardial adipose tissue is a source of inflammatory mediators. Circulation. 108(20):2460–2466.

Pham D, Xu C, Prince J. 2000. Current methods in medical image segmentation. Annu Rev Biomed Eng. 2:315–337.

Press W, Teukolsky SA, Vetterling WT, Flannery BP. 1997. Numerical recipes in C: the art of scientific computing. New York: Cambridge University Press.

Visscher TL, Seidell JC, Molarius A, van der Kuip D, Hofman A, Witteman JC. 2001. A comparison of body mass index, waist–hip ratio and waist circumference as predictors of all-cause mortality among the elderly: the Rotterdam study. Int J Obes. 25(11):1730–1735.

Yoshizumi T, Nakamura T, Yamane M, Islam A, Menju M, Yamasaki K, Arai T, Kotani K, Funahashi T, Yamashita S, Matsuzawa Y. 1999. Abdominal fat: standardized technique for measurement at CT. Radiology. 211(1):283–286.